第 18 卷 第 5 期 电化学 Vol. 18 No. 5
2012 年 10 月 JOURNAL OF ELECTROCHEMISTRY Oct. 2012

Artical ID:1006-3471(2012)05-0387-18

In situ PM-IRRAS Studies of A Floating Bilayer Lipid Membrane at Au(111) Electrode Surface

Zhangfei Su, Annia Kycia, J. Jay Leitch, Jacek Lipkowski*
(*Department of Chemistry, University of Guelph, Guelph, Ontario N1G 2W1, Canada*)

Abstract: *In situ* polarization modulation infrared reflection absorption spectroscopy (PM-IRRAS) was used to study the structure of a DMPC + cholesterol + GM1 floating bilayer lipid membrane (fBLM) at a Au(111) surface. 1-thio-β-D-glucose (β-Tg) was self-assembled onto the Au electrode to increase the overall hydrophilicity of the surface. The fBLM was then deposited on the β-Tg self-assembled monolayer (SAM) using a combination of Langmuir-Blodgett/Langmuir-Schaefer (LB/LS) techniques. The carbohydrate headgroups of the GM1 molecules were physically adsorbed to the β-Tg SAM forming a water rich cushion between the fBLM and the modified gold substrate. The PM-IRRAS spectra indicate that the DMPC molecules within the fBLM are more hydrated than previous studies involving supported bilayer lipid membranes (sBLM) where the membrane is directly adsorbed onto the surface. The tilt angle of the DMPC acyl chains in the fBLM is smaller than that of the sBLM composed of similar components. The results from this work confirmed that the fBLM is stable over a wide range of electrode potentials and that a water rich region is present between the bilayer and gold electrode surface. The addition of this water region more closely mimics the natural environment of a biological membrane making the fBLM a desirable candidate for future *in situ* studies involving transmembrane proteins.

Key words: PM-IRRAS; floating bilayer lipid membrane; Au(111) electrode; water rich region
CLC Number: O6-041 **Document Code:** A

1 Introduction

A biological membrane acts as a selective barrier that separates the interior of the cell or organelle from the external environment. As a result, the chemical environment of the intracellular fluid differs from the extracellular matrix. Biological membranes are assemblies of lipids, sugars and proteins, which are primarily held together by non-covalent interactions[1-2]. The most important feature of a biological membrane is that these structures are selectively permeable and only allow certain proteins, ions or metabolites to cross by diffusion[3-4]. Understanding the properties and functions of different cell membrane based on the composition and structure of the lipid molecules is a rapidly growing interest in multidisciplinary research around the world[5].

Supported lipid bilayer membranes (sBLM) at different substrates, including metal, silicon, mica and glass, have been employed to model the biological membranes for more than 30 years[6-7]. The sBLM is a planar bilayer with one leaflet physically adsorbed to a solid surface and the other leaflet is freely exposed to solution. The planar geometry and the long-term mechanical stability of this design allows one to investigate the relationship between the structure and properties of the bilayer using a wide range of surface sensitive techniques, such as IR spectroscopy[8], Raman[9], SPR[10], neutron reflectivity

Received: 2012-08-25; Revised: 2012-10-23 *Corresponding author, Fax: (519) 766 1499, E-mail: jlipkows@uoguelph.ca
This work was supported by Discovery grant from the Natural Sciences and Engineering Research Council of Canada. J.L. acknowledges support from the Canada Research Chairs (CRC) program.

[11], NMR[12], and XRD[13].

One of the primary drawbacks of the sBLM is the possibility of interactions between the lipid molecules and the substrate. Although sBLM generally do not directly touch the substrate surface, they are separated by a very thin water gap. The thickness of this water cushion between the solid support and the bilayer depends on the nature of the substrate and affects the overall fluidity of the lipids at the surface[14-15]. In the case of certain metal surfaces, such as gold, the lipids have nearly no lateral mobility along the surface[16], while those adsorbed to silica retain most of their fluidity since the thickness of the water layer between lipids and the surface is approximately 1 nm[14]. However, despite this separation, sBLM have lower diffusion coefficients than free-standing bilayers with the same lipid composition due to extensive hydrodynamic coupling between the bilayer and the substrate surface[17]. These interactions with the substrate are a great problem when incorporating integral membrane proteins, particularly those with large domains that extend beyond the core of the bilayer. These proteins will often become denatured and lose their functionality when in contact with the substrate surface[18].

The desire to investigate the incorporation of trans-membrane proteins in lipid bilayers under non-denaturing conditions has triggered the development of tethered bilayer lipid membranes (tBLM), in which the bilayer is separated from the substrate by a hydrophilic spacer molecule[19-20]. Gold can be used as a substrate with thiolipids due to the spontaneous formation of a covalent Au—S bond at the surface. Thiolipids are composed of lipid derivatives, extended at their polar head-groups by hydrophilic spacers, linked to extended polar head groups (i.e. hydrophilic spacers) that are terminated with a —SH group. This hydrophilic space is about several nm, hence the interaction of lipid with the substrate is minimal and the extra separation allows for the introduction of protein ion channels into the bilayer[21]. However, the tethering lipids are neither a commercially nor a naturally occurring molecules, but rather a functionalized lipid which is synthesized by a complex procedure.

Recently, a floating bilayer lipid membrane (fBLM) at SAM modified Au(111) surface was developed in this group[22]. β-Thioglucose (β-Tg) monolayer was self-assembled at the Au(111) surface, increasing the overall hydrophilicity of the surface. The fBLM, containing DMPC + cholesterol + GM1 in the inner leaflet and DMPC + cholesterol in the outer leaflet, was assembled on the β-Tg SAM using the Langmuir-Blodgett (LB) and Langmuir-Schaefer (LS) techniques. Fig. 1A shows a cartoon representation of this fBLM structure. The bilayer is separated from the modified gold surface by a water rich region, is formed by physical adsorption of the carbohaydrate headgroup of GM1 with the β-Tg SAM, preserving the natural fluidity of the lipids. The atomic force microscopy (AFM) studies[22] demonstrated that incorporating 30 mol% GM1 in the inner leaflet of the fBLM yielded the most uniform and defect-free lipid bilayer, making it an ideal model membrane for studying voltage-gated ion channels.

In situ Polarization Modulation Infrared Reflection Absorption Spectroscopy (PM-IRRAS) is a powerful technique to study adsorption of thin organic films at a metal electrode surface[23]. PM-IRRAS has high S/N and is nearly insensitive to atmospheric H_2O and CO_2. In addition, a voltage can be applied to the electrode surface while simultaneously collecting PM-IRRAS spectra. By combining the experimental PM-IRRAS spectra with theoretical calculations, the potential driven changes in the orientation and conformation of the adsorbed molecules can be studied quantitatively over a wide range of potentials. In IR spectroscopy, the amide I band (1600 ~ 1700 cm^{-1}) of the proteins does not overlap with IR absorption bands of the lipid molecules[24]; hence PM-IRRAS is ideal for the research associated with the incorporation of proteins into lipid bilayers on metal electrode surfaces[25].

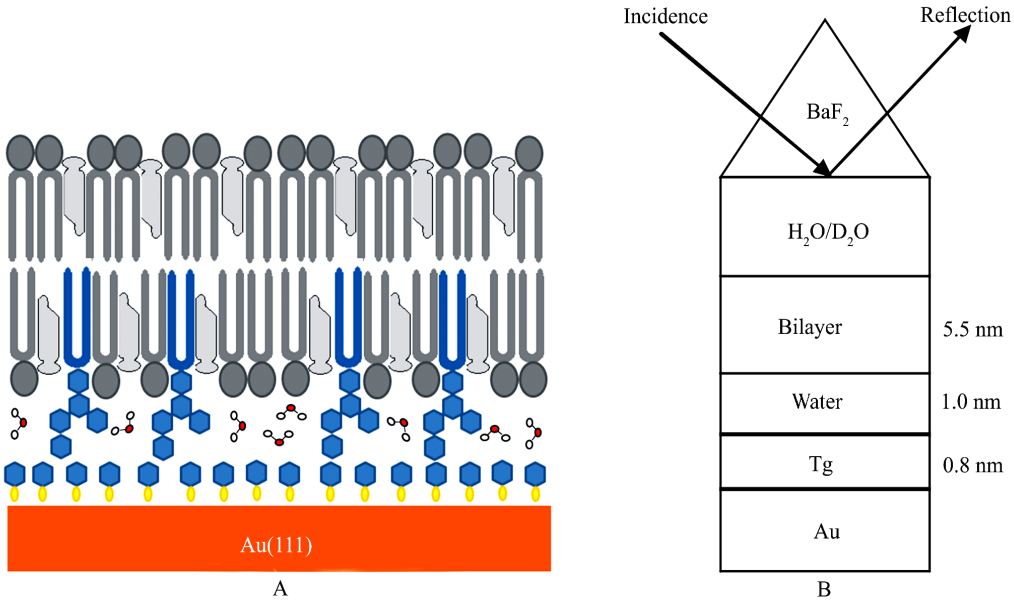

Fig. 1 A. Schematic of the fBLM on a β-Tg SAM at Au(111) surface. B. Six-layer model used in the simulation of PM-IRRAS spectra.

In this paper, *in situ* PM-IRRAS was performed to study the structure and orientation of an fBLM containing 30 mol% GM1 in the inner leaflet at different electrode potentials. Differential capacitance (DC) measurements were used to probe the stable potential region of the fBLM at the gold electrode surface. The information regarding the structure and orientation of this fBLM was obtained at different potentials and compared with previous data from sBLM models[26], which were also prepared using similar components and the LB-LS technique. In the sBLM, the leaflet with GM1 was directed towards the solution and the leaflet without GM1 was in direct contact with the Au(111) electrode surface. The results presented in this paper provided a description of the fBLM at the molecular-level, confirming that a water rich region exists between the lipid bilayer and gold substrate. This fBLM is a suitable platform for follow-up *in situ* research of voltage-gated proteins channels.

2 Experimental

2.1 Reagents, Solutions, and Electrode Materials

1,2-dimyristoyl-sn-glycerol-3-phosphocholine (DMPC, 99%), cholesterol (chol, 99%) and 1-thio-β-D-glucose sodium salt (β-Tg) were purchased from Sigma-Aldrich. Ganglioside (GM1) and 1,2-dimyristoyl (*d*54)-*sn*-glycerol-3-phosphocholine (DMPC-*d*54), in which all 54 of the acyl chain hydrogens have been replaced by deuterium, were obtained from Avanti Polar Lipids. The electrolyte for electrochemical and PM-IRRAS experiments was prepared from sodium fluoride (Sigma-Aldrich, BioXtra, 99%). The NaF powder was placed in a UV-ozone chamber (UVO cleaner, Jelight, Irvine, CA.) for 20 minutes to oxidize any organic impurities prior to use. All aqueous solutions were prepared from ultrapure water purified by a Milli-Q UV plus (Millipore, Bedford, MA) water system (resistivity > 18.2 MΩ·cm) or deuterated water (D_2O, Cambridge Isotope Laboratories, Cambridge, MA).

The single crystal Au(111) electrodes, which were grown, oriented, and cut in our laboratory, were used as the working electrodes in electrochemical and PM-IRRAS experiments. Prior to each experiment, the Au(111) electrode was flame-annealed, cooled in air, rinsed with pure water and dried over a flame. In the electrochemical experi-

ments, a saturated calomel electrode (SCE) reference electrode located in a separate compartment was connected to the cell via a Luggin capillary and a flame-annealed gold coiled wire was used as the counter electrode. In the PM-IRRAS measurements, a Pt foil and a Ag/AgCl (saturated KCl) were used as the counter and reference electrode, respectively. All potentials reported in this paper are quoted versus the Ag/AgCl (sat. KCl) reference electrode. The potential difference between the Ag/AgCl and SCE is 0.045 V. All experiments were performed at room temperature (20 ± 2 ℃) unless otherwise specified.

2.2 Self-Assembly of β-Tg at Au(111) Surface

The Au(111) electrode was flame-annealed and then immersed into a 2 mmol·L^{-1} solution of β-Tg sodium salt in methanol (Fisher Scientific, HPLC grade) for approximately 20 h. Afterwards, the electrode was thoroughly rinsed with methanol and water, and then bubbled in pure water with argon (Linde Canada, Guelph, Ontario, Canada) for approximately 1 h to remove any residual methanol and physically adsorbed β-Tg.

2.3 Bilayer Deposition

A combination of Langmuir-Blodgett (LB) and Langmuir-Schaefer (LS) techniques were employed to fabricate the fBLM on top of the β-Tg SAM at the Au(111) surface. The subphase of the Langmuir trough was heated to ~ 30 °C in order to improve the homogeneity and fluidity of the compressed film [27]. The first monolayer (inner leaflet) contained a mixture of DMPC, cholesterol and GM1 in a 40:30:30 mol% ratio. A 0.1 mol·L^{-1} HCl (Fisher Scientific) solution was used as the subphase to stabilize the GM1 molecules, which have sialic acid residues[28]. The carbohydrate headgroup of the GM1 molecules formed the hydrophilic spacer region between the β-Tg SAM and the inner leaflet. This monolayer was transferred at a surface pressure of 40 mN·m^{-1} using the LB method by vertical withdrawal of the electrode. The transfer ratio of the deposition was 1.0 ± 0.1. After the LB transfer, the monolayer-covered electrode was dried for 1.5 h. The second monolayer (outer leaflet), containing only DMPC and cholesterol in a 70:30 mol% ratio, was deposited using the LS method on a pure water subphase around 30 °C. The electrode covered by the inner leaflet was horizontally brought into contact with the DMPC/chol monolayer, which was spread and compressed to a pressure of 40 mN·m^{-1} at the trough surface, and then lifted upwards. The electrode after the LS procedure was dried for another 1.5 h before performing the electrochemical and PM-IRRAS experiments. This LB-LS method allows for the construction of an asymmetric bilayer, which contains a hydrophilic spacer region between the substrate and the inner leaflet.

2.4 Electrochemical Instrumentation and Measurements

Electrochemical measurements were carried out in an all glass three-electrode cell using a hanging meniscus configuration. The cell was de-aerated by purging with argon for 30 min. To prevent the influx of oxygen, an argon blanket was maintained over the solution throughout the experiments. The removal of oxygen from the electrolyte allows a more negative potential to be applied to the working electrode and extend the potential range where it is ideally polarized. The surface of the Au (111) electrode was carefully touched to the supporting electrolyte and slowly raised to attain a hanging-meniscus configuration. This configuration allows for measurements of only the single crystal surface, which is in contact with the electrolyte solution.

Electrochemical experiments were performed using a computer-controlled system, consisting of a potentiostat/galvanostat (HEKA PG590, Lambrecht/Pfalz, Germany) and a lock-in amplifier (EG&G Instruments 7265 DSP, Cypress, CA). The analog signals from the working electrode were transmitted to a data acquisition interface (NI-DAQ 6052E, National Instruments, ON). The DAQ board digitized the analog signals from the potentiostat and transmitted the digital signals to a computer for analysis. Custom software was used to collect elec-

trochemical data. This software was generously supplied by Prof. Dan Bizzotto, University of British Columbia, with modifications made by Prof. Ian Burgess, University of Saskatchewan.

The differential capacitance curves were determined using a scan rate of 5 mV·s^{-1} and an ac perturbation with a 25 Hz frequency and 5 mV r.m.s. amplitude. The differential capacitances were calculated from the in-phase and out-of-phase components of the ac signal assuming a simple series of RC equivalent circuit. The potentiostat settings were 100 kHz for the bandwidth and 100 kHz for the current filter. The current follower was adjusted according to the magnitude of the imaginary and real components.

2.5 PM-IRRAS Experiment

PM-IRRAS experiments were performed on a Thermo Nicolet Nexus 870 spectrometer (Madison, WI), equipped with an external tabletop optical mount (TOM) box, an MCT-A detector, a photoelastic modulator (Hinds Instruments PM-90 with a I-I/ZS50 ZnSe 50 kHz optical head, Hillsboro, OR), and a demodulator (synchronous sampling demodulator, GWC Instruments, Madison, WI). The TOM box was purged throughout the experiment using CO_2 and H_2O-free air, which was provided by a purge gas generator (Whatman, Haverhill, MA). The spectra were collected using in-house software, an Omnic macro, and a digital-to-analog converter (Omega, Stamford, CT) to control the potentiostat (EG&GPAR362, Princeton, NJ). A three-electrode electrochemical IR cell with a 1 inch BaF_2 equilateral prism (BoXin, Changchun, China) was used in the IR experiment. Prior to each experiment, the window was washed with methanol and pure water, and then cleaned for 15 min in the UV-ozone chamber. The fBLM covered gold electrode was assembled in the IR cell, which was sealed with the BaF_2 prism. The cell was filled with 0.1 mol·L^{-1} NaF electrolyte using either H_2O or D_2O to suppress the dissolution of the BaF_2. The solution was de-aerated by purging with argon for approximately 30 min to remove O_2 and an argon blanket was maintained over the solution throughout the duration of the experiment to prevent the influx of oxygen. A starting potential of E = 0.4 V was applied to the modified gold electrode, and the potential was then stepped in the negative direction via 0.1 V steps until reaching a final potential of -1.2 V. At each potential, 4000 IR scans were added and averaged using an instrumental resolution of 4 cm^{-1}.

The PM-IRRAS spectra were measured with the PEM set for half-wave retardation at 2150 cm^{-1} for the C—D stretching region, 1650 cm^{-1} for the C═O stretching region, 1400 cm^{-1} for the C—H bending region, 1250 cm^{-1} for the P—O stretching and C—H wagging region. In the 2150, 1650 and 1400 cm^{-1} regions, the angle of incidence was set to 60°, and an angle of incidence of 57° for the 1250 region. These parameters were selected to obtain a large enhancement of the mean square electric field strength (MSEFS) of p-polarized radiation at the electrode surface. A 0.1 mol·L^{-1} NaF solution in H_2O was used for the ~ 2150 cm^{-1} and ~ 1250 cm^{-1} regions, and 0.1 mol·L^{-1} NaF solution in D_2O was used for the ~ 2900 cm^{-1}, ~ 1650 cm^{-1} and ~1450 cm^{-1} regions to avoid the overlap with the strong absorption bands from the bending and stretching of H_2O and D_2O molecules, respectively. The thickness of the thin layer cavity between the electrode surface and the IR transparent prism was determined by comparing the experimental reflectivity spectrum of the thin layer cell, which is attenuated due to the absorption of solvent within the cavity, to the reflectivity spectrum calculated from the optical constants of the cell constituents as described in ref.[29].

The demodulation technique developed by Corn's group was used in this work[30]. After demodulation, two signals were measured: the average intensity $I_A(\omega)$ and the difference intensity $I_D(\omega)$. A modified version of the method described by Buffeteau et al.[31-32] was used to correct the $I_A(\omega)$ and $I_D(\omega)$ for the PEM response functions and differences in the optical throughputs of p-and s-polarized radiation. These corrections were performed separately for each spectral region using PEM functions

that were measured at conditions identical to those used for spectral acquisition. The details of these calculations are described in ref.[33]. After these corrections, the PM-IRRAS spectra contain the absorption of the IR radiation by both the adsorbed molecules on electrode surface and the background absorption due to the electrolyte in the thin layer cavity. A spline interpolation technique described by Zamlynny et al.[34] was used to subtract this background absorption. The same wavenumber range was used to construct the baseline for all of the spectra. After applying all of these corrections, the signal plots ΔS, which is proportional to the absorbance A of the molecules adsorbed on the electrode surface and is defined as:

$$\Delta S = \frac{2\,(I_s - I_p)}{I_s + I_p} = 2.3\,A = 2.3\,\Gamma\,\varepsilon \qquad (1)$$

where I_s and I_p are the intensities of s- and p-polarized radiation, Γ is the surface concentration of the adsorbed species and ε is the decimal molar absorption coefficient of the adsorbed species.

2.6 Simulation of the PM-IRRAS Spectra

The PM-IRRAS spectra of the fBLM can be simulated according to a model of six homogeneous, parallel phases (Au/β-Tg/water/bilayer/H_2O[or D_2O]/BaF_2) using custom made software that solves the Fresnel equations using the transfer matrix method[34]. The model of these phases is shown in Fig. 1B. The first layer is the gold substrate and the second layer is β-Tg SAM. Since a water rich region is formed between the β-Tg SAM and the bilayer during the LB-LS assembly, the third layer in the model is water. The fourth layer consists of the bilayer, which contains DMPC/chol/GM1. The fifth layer is either H_2O or D_2O, depending on the IR experimental region, and the final layer is the BaF_2 prism. The optical constants of gold, H_2O, D_2O and BaF_2 can be obtained from literature[35-37]. The optical constants of β-Tg was measured from the FTIR transmission experiment of β-Tg sodium salt in H_2O or D_2O solution, and the optical constant of the DMPC/chol/GM1 mixture was determined from the FTIR transmission experiment of DMPC/chol/GM1 vesicles in H_2O or D_2O. The detailed description of the measurement of the optical constants is given in ref.[33]. Although in the actual system, the concentration of DMPC/chol/GM1 in the inner and outer leaflet is different, in the simulation, these two leaflets were treated as a homogeneous layer. The concentration of DMPC/chol/GM1 in the forth layer was the average value of the two leaflets (55 mol% DMPC, 30 mol% chol, and 15 mol% GM1). Based on the literature and previous results from our group[38-40], the thickness of the β-Tg SAM layer was set as 0.8 nm and the thickness of the bilayer (without GM1 headgroup) was set as 5.5 nm. According to the recent AFM results[22], the thickness of the fBLM containing 30% of GM1 is about 7.3 nm. Hence the thickness of the third water layer is calculated to be about 1.0 nm.

3 Results and Discussion

3.1 Differential Capacitance Measurements

The compactness of the fBLM and the number of defects in the membrane can be evaluated by measuring the differential capacitance. According to the Helmholtz model, the interface between the electrolyte solution and the electrode behaves as a capacitor, where the capacitance of the interface, C_d, is given by:

$$C_d = \frac{\varepsilon_r\,\varepsilon_0}{d} \qquad (2)$$

where ε_o is the permittivity of free space, ε_r is the relative permittivity of the medium and d is the thickness of the capacitor. A perfect, defect-free bilayer is characterized by a low permittivity ($\varepsilon_r \approx 2$), which is indicative of the lipid molecules. In the presence of defects, water molecules penetrate into the bilayer, and as a result its permittivity increases, which leads to an overall increase in the capacitance. Therefore, the measurement of the capacitance is a convenient means to investigate the compactness of the bilayer. In addition, the capacitance can be measured as a function of the electrode potential and used to monitor the effect of the electrode potential on the bilayer structure.

In the case of fBLM deposited at Au(111) sur-

face modified by a hydrophilic SAM, we expect to have water trapped between the lipid bilayer and the gold surface. How will this trapped water affect the total capacitance being measured? An electrical model of the fBLM system is shown in Fig. 2A. The membrane capacitance (C_M) is in series with an effective Helmholtz capacitance (C_H) due to the ionic double layer next to the gold surface. The total capacitance of a nonconductive fBLM is therefore $C = C_M C_H /(C_M + C_H)$. Based on Eq. 2, the magnitude of the capacitance is controlled by permittivity and the thickness of the capacitor. Fig. 1 shows that the thickness of the Helmholtz (water reservoir plus monolayer of thioglucose) and membrane are approximately 1.8 and 5.5 nm, respectively. However, since the permittivity of C_H is much larger compared to the permittivity of C_M ($\varepsilon_H >> \varepsilon_M$), we can approximate that the value of $C_H >> C_M$ such that the contribution of C_H to the overall capacitance can be considered negligible and thus $C \approx C_M$.

Raguse et al. [41] performed impedance spectroscopy studies on a tBLM and found that the C_H value in the assembled bilayer system (5 $\mu F \cdot cm^{-2}$) is smaller than the Helmholtz capacitance of a bilayer-free gold surface (20 $\mu F \cdot cm^{-2}$). They suggested this difference in C_H is due to the presence of the sulfur/reservoir groups partially blocking the surface or by the organization of water within the reservoir region due to the ethylene oxide tether, which causes the dielectric constant within the reservoir region to be lower than that of the bulk aqueous solution[41]. This is probably a similar situation for the fBLM in this work, with respect to the carbohydrate headgroup of GM1. However, C_H would only contribute approximately 10 ~ 20% to the total capacitance such that the above approximation ($C \approx C_M$) is still valid.

Fig. 2B plots the differential capacitance of the film-free Au(111) electrode, the electrode covered by β-Tg SAM, and of the fBLM containing 30 mol% GM1 in the inner leaflet deposited on the β-Tg modified electrode. As shown in Fig. 2B, the bilayer is very stable within the potential window from 0.5 V to -0.1 V (vs. Ag/AgCl). As the potential is swept to more negative values, a phase transition occurs (observed as the peak) corresponding to the bilayer being lifted from the β-Tg modified gold electrode surface. At very negative potentials (< -1.0 V), the capacitance curve merges with that of bare Au(111) surface, demonstrating that the fBLM and β-Tg SAM are completely lifted from the Au(111) [42]. Neutron reflectivity experiments described in ref.[42] demonstrated that in the lifted state the bilayer remains in a close proximity to the electrode separated by a thin cushion of the electrolyte. In the potential region at which the fBLMs are stable (E = 0.5 to -0.1 V), the minimum value of the capacitance is 2.2 $\mu F \cdot cm^{-2}$. Although this value is much lower than the minimum capacitance of the electrode covered by the β-Tg (12.8 $\mu F \cdot cm^{-2}$), it is still higher than the capacitance of a biological membrane which is ~ 1.0 $\mu F \cdot cm^{-2}$[43]. These results imply that a fBLM containing 30 mol% GM1 in the inner leaflet may contain multiple defects. However, these results indicate that an electrochemically stable bilayer is produced, even though it is only physically adsorbed to the surface. In addition, this low value of the capacity indicates that the hydrated layer separating the membrane from the metal does not contain electrolyte. At negative potentials, where the bilayer is lifted and electrolyte flows into the region between the membrane and the metal, the potential drop across the interface takes place within the hydrated layer. Consequently, the capacitance of the electrode initially covered by the membrane becomes equal to the capacitance of the electrode that is membrane free. To differentiate between the two states we will refer to them as: “lifted” or “desorbed” if the water layer separating the membrane from the metal contains electrolyte and “adsorbed” when the water rich region is electrolyte-free. We would like to emphasize that the above measurements were performed using single frequency of the ac perturbation. Such measurements are sufficient to provide estimate of the membrane capacitance and the po tential range where the membrane is stable. However, they

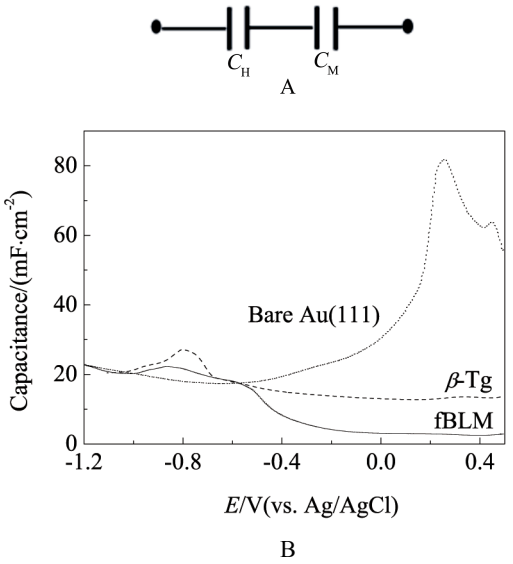

Fig. 2 A. An electric circuit describing the overall capacitance (C) as two capacitors in series: the Helmholtz capacitance (C_H) and membrane capacitance (C_M). B. Differential capacity curves of the fBLM (solid line), β-Tg SAM (dash line) and bare Au(111) (dotted line) in 0.1 mol·L^{-1} NaF/H_2O solution.

do not provide information about the membrane resistance.

3.2 PM-IRRAS Results

3.2.1 Acyl Chain Region

The C—H stretching region, located between 2800 and 3000 cm^{-1}, provides valuable information regarding the conformation and orientation of the lipid acyl chains in the BLM. However, in our fBLM, cholesterol, GM1, and β-Tg all have IR absorption in this region, which disturbs the quantitative analysis of the acyl chain of DMPC molecules. Hence, in this work, DMPC-*d*54 is used to probe the conformation and orientation of the acyl chains in the fBLM. The IR absorption of C—D stretching is located in the region between 2000 and 2300 cm^{-1}, which do not overlap with any other vibrations of the fBLM components and β-Tg SAM. The DMPC-*d*54 PM-IRRAS experiments were performed around 18 °C, below the main phase transition temperature of the lipid, which is 20.5 °C. Fig. 3A shows the PM-IRRAS spectra of the fBLM prepared by DMPC-*d*54/chol/GM1 at selected potentials and the simulated IR absorption. It can be seen that the peak intensity is changing as a function of electrode potential, demonstrating a potential-induced reorientation of the acyl chains within the fBLM. Fig. 3B shows the band deconvolution (Lorentzian fit) of the C—D stretching region along with assignment of the bands. In the deconvoluted spectrum, four bands corresponding to the CD_3 asymmetric stretching ($\nu_{as}(CD_3)$ at ~ 2216 cm^{-1}), CD_2 asymmetric stretching ($\nu_{as}(CD_2)$ at ~ 2196 cm^{-1}), CD_3 symmetric stretching ($\nu_s(CD_3)$ at ~ 2154 cm^{-1}) and CD_2 symmetric stretching ($\nu_s(CD_2)$ at ~ 2090 cm^{-1}) can be found. The two shoulder peaks on the higher frequency and lower frequency sides of the $\nu_s(CD_2)$ band correspond to Fermi resonance between CD_3 and CD_2[44-45].

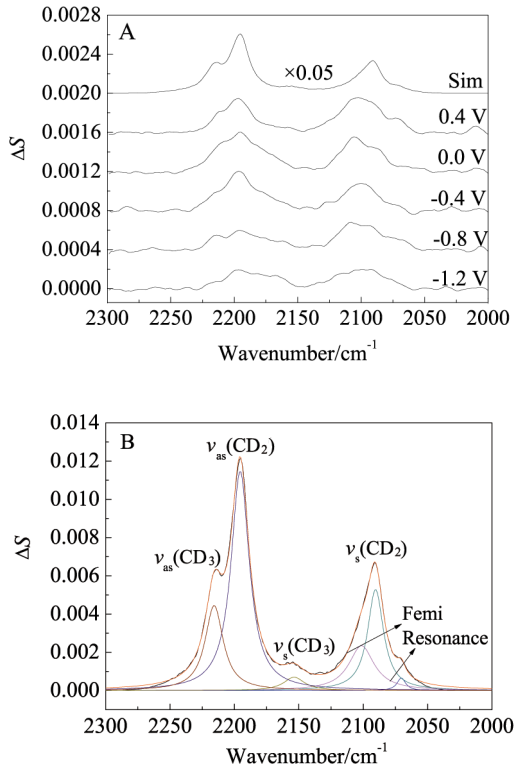

Fig. 3 A. PM-IRRAS spectra of the fBLM (composed of DMPC-*d*54) at Au (111) surface in the C—D stretching region in 0.1 mol·L^{-1} NaF/H_2O solution at selected potentials. Top line is the simulated spectrum according to the six-layer model. B. Deconvolution result of the C—D stretching bands for the simulated spectrum shown in the top line of Fig. 3A (Lorentzian fit).

Fig. 4A plots the frequencies of peak centers of the $v_{as}(CD_2)$ and $v_s(CD_2)$ bands as a function of the electrode potential. Their values are potential independent, and the average values of the peak centers of the $v_{as}(CD_2)$ and $v_s(CD_2)$ bands are ~ 2196 and ~ 2099 cm^{-1}, respectively. According to literature results[45], when DMPC-*d*54 molecules are cooled to 10 °C, which is far below the main phase transition temperature, the acyl chains are in the all-*trans* conformation and the corresponding peak centers of these two bands are located at 2191 and 2088 cm^{-1}, respectively. The frequencies reported in Fig. 4A are significantly higher suggesting that acyl chains in the fBLM are partially melted and have a certain number of *gauche* conformers. The increase in the number of *gauche* conformers is consistent with our previous results obtained for DMPC + cholesterol[46] and DMPC-*d*54 + cholesterol + GM1 [26] sBLMs, indicating that the incorporation of cholesterol and GM1 into the lipid matrix leads to an increase in the number of *gauche* conformers despite that fact that the room temperature was below the main phase transition temperature. However, Nabet et al.[47] pointed out that the frequency shift was a complex phenomenon concerning many effects such as librotorsional motions and intermolecular coupling. Therefore, the shift of the peak center cannot be exclusively explained by changes in the conformational order of the lipid acyl chains.

When linearly polarized radiation is absorbed by a sample adsorbed on electrode surface, the integrated intensity of the absorption band is proportional to the square of the absolute value of the dot product of the transition dipole vector ($\vec{\mu}$) and the electric field vector of the incident radiation ($\vec{E}$), shown as[33,48-49]:

$$\int A\,d\,v \propto \Gamma \left|\vec{\mu} \cdot \vec{E}\right| = \Gamma\,|\mu|^2\,|E|^2 \cos^2\theta \qquad (3)$$

At the metal electrode surface, the direction of the electric field vector of the *p*-polarized radiation is normal to the surface, hence the integrated band intensity in spectra of adsorbed molecules is proportional to $\cos^2\theta$, where θ is the angle between the transition dipole of the adsorbed molecule and the surface normal. For randomly oriented molecules, $\cos^2\theta = 1/3$; therefore the orientation of adsorbed species at the electrode surface can be determined from the experimental PM-IRRAS spectrum and the simulated spectrum of randomly oriented molecules according to the following relationship[48-49]:

$$\cos^2\theta = \frac{\int A_{exp}\,dv}{3\int A_{cal}\,dv} \qquad (4)$$

where A_{exp} is the experimentally measured PM-IRRAS spectrum of adsorbed species at the electrode surface and A_{cal} is the IR spectrum simulated using the isotropic optical constants. If the direction of the transition dipole moment is known, the orientation of the adsorbed molecules can be determined by relating the direction of the transition dipole moment to the geometry of the molecule. In the interpretation of the PM-IRRAS data, the absolute value of the transition dipole is assumed to be independent of the static electric field at the electrode surface, so that the changes in the band intensity can be explained by the reorientation of the molecules. This approach is widely used in the IR studies of electric field driven transformations in organic thin films at electrode surfaces[26,46,50-51].

For the CD_2 asymmetric stretching vibration, the direction of the transition dipole lies along the line joining the two deuterium atoms of the CD_2 group, while for the CD_2 symmetric stretching, the direction of the transition dipole lies along the bisector of the CD_2 plane. Both of the vectors are orthogonal to each other and form a 90° angle with the line of a fully extended all-*trans* hydrocarbon chain. Therefore, the angles $\theta_{as}(CD_2)$ and $\theta_s(CD_2)$ and the average tilt angle of trans fragments of the DMPC hydrocarbon chain (θ_{chain}) are related by the equation[52]:

$$\cos^2\theta_{as} + \cos^2\theta_s + \cos^2\theta_{chain} = 1 \qquad (5)$$

The $\theta_{as}(CD_2)$ and $\theta_s(CD_2)$ can be calculated according to Eq. 4 from the integrated intensity of CD_2 asymmetric and symmetric stretching bands in the experimental and simulated spectra.

Fig. 4B shows the average tilt of *trans* fragments of the acyl chain of DMPC molecule in the

fBLM as a function of electrode potential. For comparison the tilt of the *trans* fragments of the sBLM[26] with the same composition is also included in Fig. 4B. The tilt angles reported in the present work are the average orientation of DMPC molecules in both leaflets of the bilayer. It can be seen that in the adsorption state, the tilt angle of the fBLM is nearly potential-independent, and the average value is ~ 12 ± 1°. At very negative potentials, where the fBLM is desorbed from the Au(111) surface, the tilt angle decreases to a value ~ 9 ± 1°. Similar trend is displayed by curve 2 in Fig. 4B for the sBLM in which the three component monolayer (DMPC-*d*54/cholesterol/GM1) constituted the distal leaflet (solution-side) of the bilayer. However, the average value of the tilt angle of the fBLM (~ 12°) is ~ 5° lower than that of the sBLM (~ 17°). In the adsorbed state of sBLM, the DMPC molecules in the proximal leaflet are in direct contact with the metal and the polar heads of DMPC molecules are located in a single plane. In contrast, the fBLM both leaflets are exposed to water and the bilayer is separated from the metal by a water rich layer, which allows the polar heads of the phospholipid molecules to organize in a zigzag conformation creating a more tightly packed bilayer[51,53]. Hence the tilt angle of the acyl chains is smaller in fBLM than in the sBLM. This result is consistent with recent AFM studies [22] of the same fBLM that showed that the acyl chains of the DMPC molecules in the fBLM are very tightly packed leading to formation of a thick bilayer.

3.2.2 Glycerol Ester Group

The C═O of the glycerol ester group in DMPC molecules is located at ~ 1730 cm^{-1}, providing unique information concerning the hydration of the carbonyl group. Fig. 5A shows the PM-IRRAS spectra at different potentials and simulated spectrum of the fBLM at the Au(111) surface. It can be observed that the band intensity is similar for all electrode potentials, however, the peak center shifts with the variation in potential. The weak shoulder at ~ 1710 cm^{-1} corresponds to absorption of GM1 molecules. In this paper, we discuss only the υ(C═O) band associated with DMPC molecules. The ester C═O band located at ~ 1730 cm^{-1} is quite complex. DMPC molecules have two conformers, DMPC-A (80%) and DMPC-B (20%)[54]. The normal coordinate simulation by Bin et al.[50] shows that vibrations of the υ(C═O) band in the β and γ acyl chains are coupled, causing the band to split into two bands corresponding to the in-phase and out-of-phase motion of the atoms. In the case of the predominant DMPC-A conformation, the coupling is weak, and the in-phase and out-of-phase components are separated by 5 cm^{-1}. The transition dipoles of these bands are almost normal to the acyl chains.

The position of the υ(C═O) band depends on the hydration state of the ester group. In hydrated

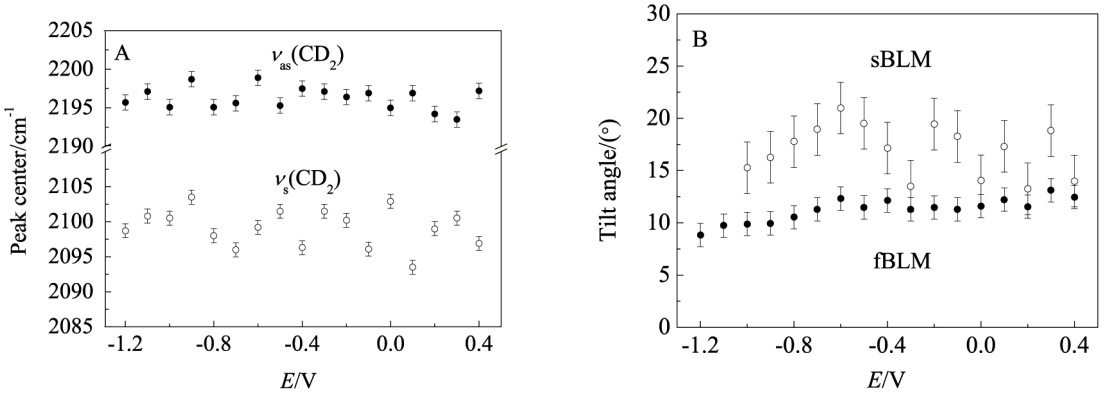

Fig. 4 A. Peak center of the $\nu_{as}(CD_2)$ (filled circles) and $\nu_s(CD_2)$ (open circles) vibrations in the deconvoluted spectra as a function of electrode potential. B. Tilt angle of the acyl chains of DMPC molecules in the fBLM (filled circles) and sBLM[26] (open circles).

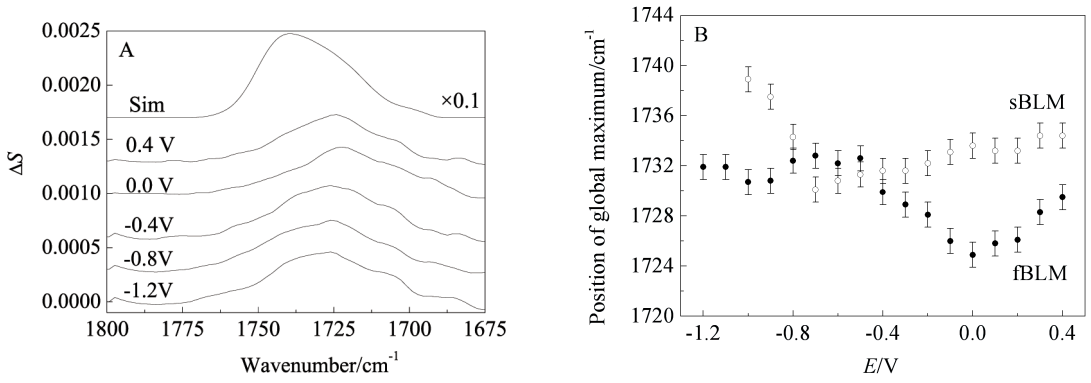

Fig. 5 A. PM-IRRAS spectra of the fBLM at Au(111) surface in the ν(C=O) region in 0.1 mol·L^{-1} NaF/D_2O solution at selected potentials. Top line is the simulated spectrum. B. Position of the global maximum of the C═O stretching band in the fBLM (close circles) and sBLM[26] (open circles) as a function of electrode potential.

phospholipids, this band splits into two components with maxima at ~ 1744 cm^{-1} and ~ 1734 cm^{-1}, corresponding to the non-hydrogen-bonded and hydrogen-bonded ν(C═O), respectively[55]. Due to the complex nature of this band in DMPC, it was not deconvoluted into the hydrogen-bonded and non-hydrogen-bonded components in this study. Instead, Fig. 5B plots the position of the global maximum of the C═O band in the fBLM and sBLM[26] as a function of the electrode potential. The minimum in the C═O peak position of the fBLM was observed at a potential of 0.0 V, which corresponds to the adsorbed state. In contrast, the minimum for the sBLM was observed at a potential of -0.8 V corresponding to the onset of the desorbed (lifted) state. This behavior illustrates a potential-induced change in the hydration of the carbonyl group. For both bilayers the position of the global maximum has lower value when the bilayer is adsorbed than when it is completely lifted from the surface, particularly in the case of the fBLM. Comparing to the global maximum in the fBLM and sBLM, we can find that for most electrode potentials, the position of the global maximum in the fBLM is smaller than that in the sBLM, demonstrating that DMPC molecules are more hydrated in the fBLM than in the sBLM. In the sBLM, the bilayer is directly deposited at a gold substrate, while in the fBLM, the bilayer is deposited on a β-Tg SAM, forming a water rich region between bilayer and substrate. Apparently, this water rich region increases the hydration of the polar head region of DMPC molecules in the fBLM. This is an important result, because these PM-IRRAS spectra for the C═O region confirm the existent of a water rich region between the fBLM and the gold surface.

Within the experimental uncertainty, the intensity of the ν(C═O) band is similar at different electrode potentials, demonstrating that the orientation of the C═O group does not change with the electrode potential. It is difficult to determine the angle between the transition dipole of ν(C═O) and the surface normal for this vibration due to the complex nature and significant changes in the hydration state of the C═O bond, however, it should be noted that the band intensity in the simulated spectrum is about 20 times greater than that in the PM-IRRAS spectra. This implies that the angle between the transition dipole of the C═O stretching and the surface normal is very large and by using the total band intensity, as a rough estimate, the angle of the transition dipole moment with respect to the surface normal was found to be ~ 87°. Since the direction of the transition dipole of the ν(C═O) band is nearly normal to the acyl chains, the large angle between the transition dipole of ν(C═O) and the surface normal is consistent with the small tilt angle of the acyl chains.

3.2.3 Choline Group

Information concerning the choline group (—CH_2—CH_2—$N^+(CH_3)_3$) can be found in the 1500

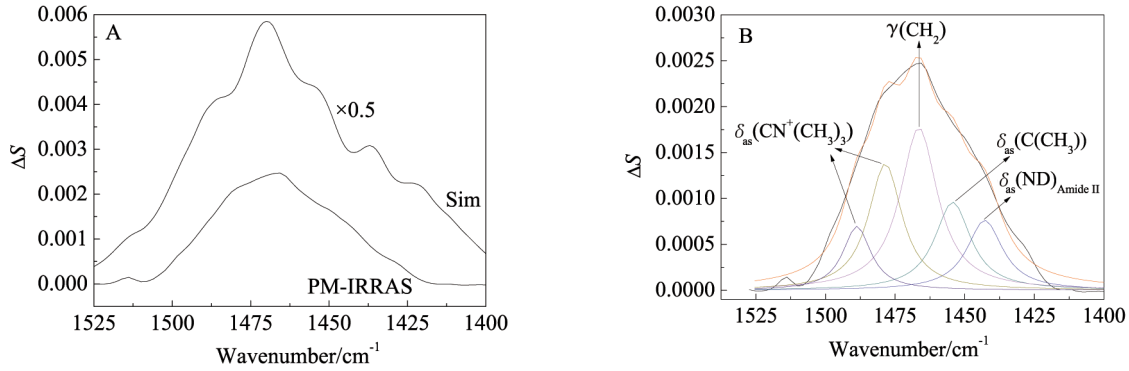

Fig. 6 A. PM-IRRAS and simulated spectra of the fBLM at Au(111) surface in the C—H bending region in 0.1 mol·L^{-1} NaF/D_2O solution. The PM-IRRAS spectrum is averaged for all potentials. B. Deconvolution result of the C—H bending region (Lorentzian fit).

to 1350 cm^{-1} region for the C—H bending mode and 1000 to 850 cm^{-1} region for the C—N stretching bands. The second region also contains bands from the sugar rings of β-Tg and GM1 and interpretation of that spectral region is very difficult. Therefore we will discuss only the choline group spectra in the 1500 to 1350 cm^{-1} region. Fig. 6A shows the PM-IRRAS and simulated spectra of the fBLM at the Au(111) surface in the C—H bending region. The PM-IRRAS spectra of the fBLM in this region at different potentials are given in Fig. S1 in the Supplementary material. The features of these IR bands appear to be independent of the electrode potential. Therefore, to improve the signal to noise ratio, the PM-IRRAS spectra at each potential was averaged, with the resulting spectrum shown in Fig. 6A. Since the choline group is poorly hydrated, the differences between experimental and simulated spectra are chiefly affected by the change in orientation. The $\delta_{as}(CN^+(CH_3)_3)$ bands appear at ~ 1480 and ~ 1490 cm^{-1}, while the $\delta_s(CN^+(CH_3)_3)$ bands are located at ~ 1380 and ~ 1420 cm^{-1}. The symmetric bands are much weaker and difficult to distinguish from the background in the PM-IRRAS spectra, as a result we will only discuss the asymmetric bands. Fig. 6B illustrates the deconvoluted spectrum in the C—H bending region, in which two peaks in 1479 and 1489 cm^{-1} are assigned to the $\delta_{as}(CN^+(CH_3)_3)$ vibration. Besides these two bands, three bands located in 1466, 1454, 1443 cm^{-1} are attributed to $\gamma(CH_2)$, $\delta_{as}(C(CH_3))$, and $\delta_{as}(ND)_{Amide\ II}$ respectively[56-58].

The direction of the transition dipoles of the choline group has been discussed thoroughly by Fringeli[56-58]. The $CN(CH_3)_3$ fragment has a C_{3v} symmetry. The symmetry of $\delta_{as}(CN^+(CH_3)_3)$ band at 1489 cm^{-1} was classified as A1. For this vibration direction of the transition dipole is parallel to the C_3 axis of the choline group. The symmetry of 1479 cm^{-1} band was classified as E. For this vibration direction of the transition dipole is perpendicular to the C_3 axis and is located in the plane of the three methyl groups. The angles between the transition dipoles of $\delta_{as}(CN^+(CH_3)_3)$ and the surface normal can be determined by Eq. 4. The average values of the angles are calculated to be ~ 84 ± 1° for the 1489 cm^{-1} band and ~ 85 ± 1° for the 1479 cm^{-1} band. As shown in Fig. S1, the band intensity changes randomly with potential. The spread of the band intensity reflects chiefly the uncertainty of the background correction procedure. Therefore, the error bar was calculated according to the spread of the band intensity over potentials. The values of these angles are very large and are independent of the electrode potential. The tilt angle of the C—N bond in the fBLM is about 10° higher than that in the sBLM[26] with similar components, indicating that the β-Tg SAM affects the orientation of the polar headgroups in the bilayer lipid membrane.

3.2.4 Phosphate Group

The IR absorption of the phosphate group

contains the $\nu_{as}(PO_2^-)$ at ~ 1225 cm^{-1} and $\nu_s(PO_2^-)$ at ~ 1090 cm^{-1} of the PO_2^- moiety, and two bands corresponding to ν_{as}(C-O[P]) of the phosphate ester group between 1050 cm^{-1} to 1100 cm^{-1} [56-58]. As we have mentioned above, the ν_{as}(C-O[P]) and $\nu_s(PO_2^-)$ overlap with other absorption bands in the 900 ~ 1200 cm^{-1} region and is too difficult to deconvolute bands in this region. As a result, we only discuss the $\nu_{as}(PO_2^-)$ band. Fig. 7A shows the PM-IRRAS and simulated spectrum of the fBLM in the $\nu_{as}(PO_2^-)$ region. The PM-IRRAS spectra of the fBLM in this region at different potentials are shown in Fig. S2 of the Supplementary material. It can be observed that the features of this IR band are potential independent. Fig. 7B shows the deconvoluted PM-IRRAS spectrum. It can be observed that the IR absorption in this region involves four bands, CH_2 wagging at ~ 1277 cm^{-1}, Amide III at 1244 cm^{-1}, $\nu_{as}(PO_2^-)$ at ~ 1222 cm^{-1}, and $\nu_{as}(C\text{-}O\text{-}C)_{ester}$ at ~ 1205 cm^{-1}. The peak center of the $\nu_{as}(PO_2^-)$ band in the simulated spectrum is located at ~ 1233 cm^{-1}. This band is composed of two components, a hydrogen-bonded component at ~ 1221 cm^{-1} and a non-hydrogen-bonded component at ~ 1239 cm^{-1}[59]. Compared to the simulated result, the peak center of the $\nu_{as}(PO_2^-)$ band in the experimental spectrum is red shifted by ~ 11 cm^{-1}, which indicates a dramatic increase in the hydration state of DMPC molecules in the fBLM compared to the vesicle dispersion. The peak center of the $\nu_{as}(PO_2^-)$ band for the fBLM is also ~ 6 cm^{-1} smaller than for the sBLM[26], demonstrating that the fBLM has a greater hydrogen-bonded component than the sBLM. This result reinforces that a water rich region exists between the bilayer and substrate. Since the inner leaflet of the fBLM was fabricated on 0.1 mol·L^{-1} HCl subphase, the PO_4^- group could be protonated during the LB procedure. However before the PM-IRRAS measurement, the system was bubbled with argon for about 5 h, which is long enough for PO_4^- group to deprotonated in NaF solution with pH ~ 8.4.

The angle between the direction of the transition dipole of the $\nu_{as}(PO_2^-)$ and the surface normal can be determined according to Eq. 4. The direction of the transition dipole of the $\nu_{as}(PO_2^-)$ vibration is parallel to the line connecting the two non-esterified oxygen atoms of the phosphate group. The angle between the transition dipole of the $\nu_{as}(PO_2^-)$ and the surface normal ($\theta_{as}(PO_2^-)$) averaged over all potentials is 71 ± 3°, which is close to that observed in the sBLM[26], illustrating that the β-Tg SAM only influences the hydrogen state of the bilayer, but does not affects the orientation of the phosphate group of DMPC molecules.

4 Conclusions

The conformation, hydration and orientation of an fBLM containing DMCP/chol/GM1 at a β-Tg modified Au(111) surface was probed *in situ* using PM-IRRAS. The lipid bilayer was assembled on a β-Tg SAM modified Au(111) surface employing

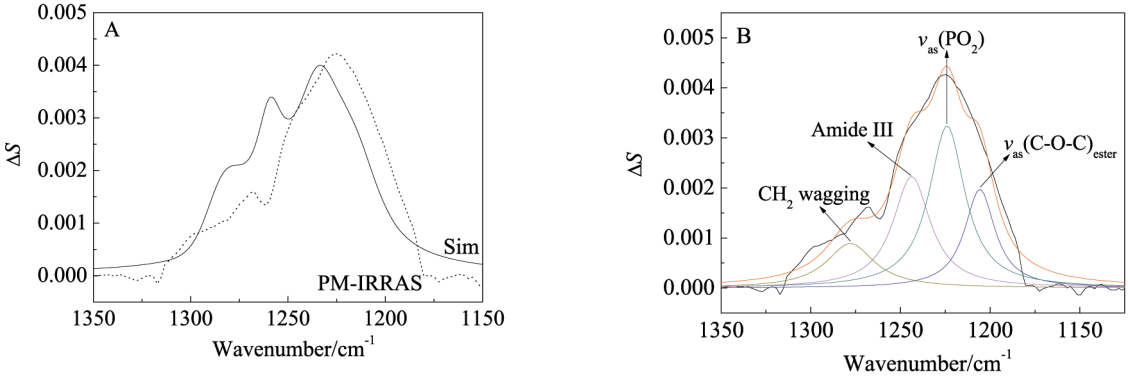

Fig. 7 A. PM-IRRAS and simulated spectra of the fBLM at Au(111) surface in the $\nu_{as}(PO_2^-)$ region in 0.1 mol·L^{-1} NaF/H_2O solution. The PM-IRRAS spectrum is averaged for all potentials. B. Deconvolution result of the $\nu_{as}(PO_2^-)$ region (Lorentzian fit).

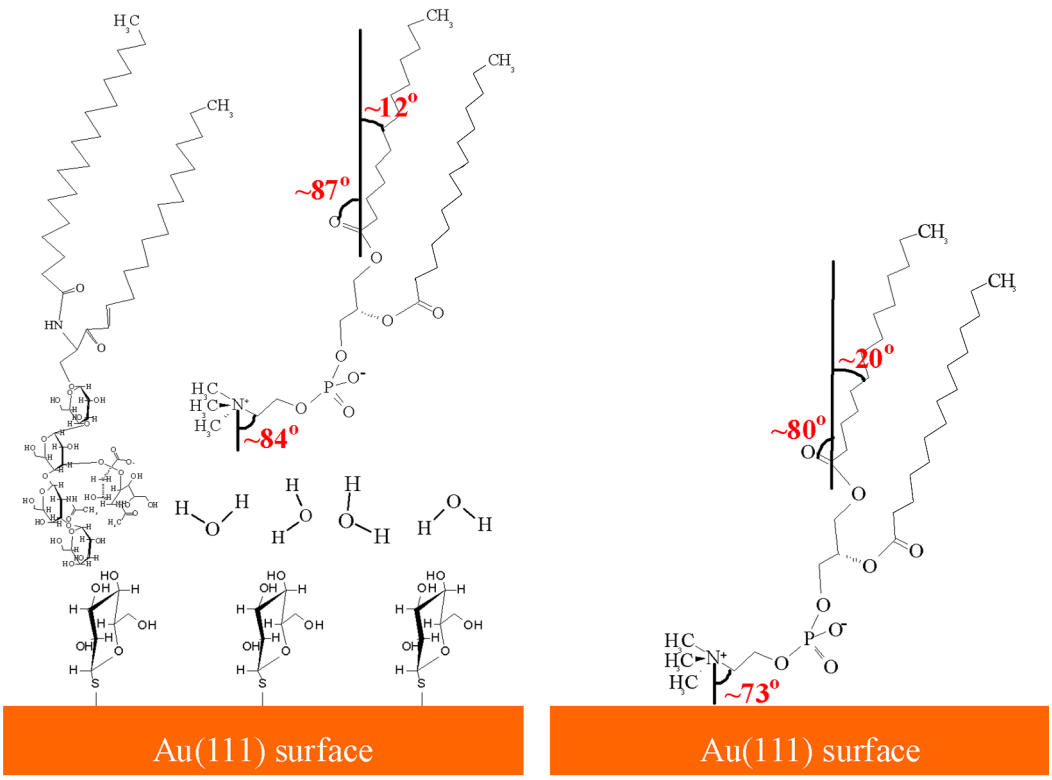

Fig. 8 Orientation of DMPC molecules in the fBLM (A) and sBLM (B)[26] at Au(111) surface in the adsorption state. This represents the average orientation of DMPC molecules in the two leaflets of the bilayer with respect to the normal of Au(111) surface.

combined LB/LS techniques. The differential capacitance curves demonstrated that the fBLM was stable at the modified-Au(111) surface over a wide potential region. Based on PM-IRRAS data, the β-Tg SAM increases the overall hydrophilicity of the surface and together with the hydrophilic carbohydrate head group of GM1 molecules forms a water rich region between lipid bilayer and gold substrate. The results obtained in the present work were compared with those for the sBLM prepared by the same method using similar membrane components. This comparison demonstrated that the polar head region of fBLM is more hydrated than than in the sBLM. Fig. 8 shows the orientation of DMPC molecules in the fBLM (A) and sBLM (B) at the Au(111) surface in the adsorption state of the bilayer. The tilt angle of the acyl chains of DMPC molecules in the fBLM is around 12 ± 1.1°, which is smaller than that in the sBLM. In the adsorbed state, the tilt angle of the acyl chains in the fBLM is larger than that in the desorbed state. The tilt angle of the C═O bond in the glycerol ester group and C—N bond in the choline group are both larger in fBLM than in the sBLM.

The PM-IRRAS and the electrochemical data confirm that the fBLM is stable at the Au(111) surface with a water rich region existing between the lipid bilayer and substrate. The water rich layer is thick enough to accommodate large transmembrane proteins and prevent denaturation and maintain protein function. The potential region in which the fBLM is stable can be used to control the open and closed state of voltage-gated ion channel proteins incorporated in the fBLM. The structural changes of these proteins at different potentials can be monitored using this model membrane. Therefore, this fBLM should be an ideal platform for future voltage-gated ion channel protein research.

Acknowledgements

The authors acknowledge many helpful discussions with Vlad Zamlynny concerning PM-IRRAS

data procesing. This work was supported by Discovery grant from the Natural Sciences and Engineering Research Council of Canada. J.L. acknowledges support from the Canada Research Chairs (CRC) program.

Supporting Information Available:

PM-IRRAS spectra of the fBLM in the C—H bending (Fig. S1) and $v_s(PO_2^-)$ region (Fig. S2) at selected potentials are available in the supplementary materials. The supporting information is available free of charge via the internet at http://electrochem.xmu.edu.cn.

References:

[1] Singer S J, Nicolson G L. The fluid mosaic model of the structure of cell membranes[J]. Science, 1972, 175 (4023): 720-731.

[2] Alberts B, Johnson A, Lewis J, et al. Molecular biology of the cell[M]. 5th Edition. New York: Garland Science, 2007: 617-650.

[3] Papahadjopoulos D, Watkins J C. Phospholipid model membranes. I. Structural characteristics of hydrated liquid crystals[J]. Biochimica et Biophysica Acta, 1967, 135 (4): 624-638.

[4] Hauser H, Phillips M C, Stubbs M. Ion permeability of phospholipid bilayers[J]. Nature, 1972, 239: 342-344.

[5] Nagle J F, Tristram-Nagle S. Structure of lipid bilayers [J]. Biochimica et Biophysica Acta, 2000, 1469 (3): 159-195.

[6] Sackmann E. Supported membranes: Scientific and practical applications[J]. Science, 1996, 271(5245): 43-48.

[7] Castellana E T, Cremer P S. Solid supported lipid bilayers: From biophysical studies to sensor design[J]. Surface Science Reports, 2006, 61(10): 429-444.

[8] Mendelsohn R, Mao G, Flach C R. Infrared reflection-absorption spectroscopy: Principles and applications to lipid-protein interaction in Langmuir films[J]. Biochimica et Biophysica Acta, 2010, 1798(4): 788-800.

[9] Lee C S, Bain C D. Raman spectra of planar supported lipid bilayers[J]. Biochimica et Biophysica Acta, 2005, 1711(1): 59-71.

[10] Lirtsman V, Ziblat R, Golosovsky M, et al. Surface-plasmon resonance with infrared excitation: Studies of phospholipid membrane growth[J]. Journal of Applied Physics, 2005, 98(9): 093506.

[11] Dabkowska A P, Fragneto G, Hughes A V, et al. Specular Neutron reflectivity studies of the interaction of cytochrome c with supported phosphatidylcholine bilayers doped with phosphotidylserine[J]. Langmuir, 2009, 25 (7): 4203-4210.

[12] Nomura K, Inaba T, Morigaki K, et al. Interaction of lipopolysaccharide and phospholipid in mixed membranes: Solid-state ^{31}P-NMR spectroscopic and microscopic investigations[J]. Biophysical Journal, 2008, 95 (3): 1226-1238.

[13] Miller C E, Majewski J, Watkins E B, et al. Probing the local order of single phospholipid membranes using grazing incidence X-ray diffraction[J]. Physical Review Letters, 2008, 100(5): 058103.

[14] Tamm L K, McConnell H M. Supported phospholipid bilayers[J]. Biophysical Journal, 1985, 47(1): 105-113.

[15] Tamm L K. Lateral diffusion and fluorescence microscope studies on a monoclonal antibody specifically bound to supported phospholipid bilayers[J]. Biochemistry, 1988, 27(5): 1450-1457.

[16] Groves J T, Ulman N, Cremer P S, et al. Substrate-membrane interactions: Mechanisms for imposing patterns on a fluid bilayer membrane[J]. Langmuir, 1998, 14(12): 3347-3350.

[17] Kuhner M, Tampe R, Sackmann E. Lipid mono- and bilayer supported on polymer films: Composite polymer-lipid films on solid substrates[J]. Biophysical Journal, 1994, 67(1): 217-226.

[18] Guidelli R, Aloisi G, Becucci L, et al. Bioelectrochemistry at metal/water interfaces[J]. Journal of Electroanalytical Chemistry, 2001, 504(1): 1-28.

[19] Lang H, Duschl C, Vogel H. A new class of thiolipids for the attachment of lipid bilayers on gold surfaces[J]. Langmuir, 1994, 10 (1): 197-210.

[20] Rossi C, Chopineau J. Biomimetic tethered lipid membranes designed for membrane-protein interaction studies[J]. European Biophysics Journal, 2007, 36 (8): 955-965.

[21] Naumann R, Jonczyk A, Kopp R. et al. Incorporation of membrane proteins in solid-supported lipid layers [J]. Angewandte Chemie International Edition, 1995, 34 (18): 2056-2058.

[22] Kycia A H, Wang J P, Merrill A R, et al. Atomic force microscopy studies of a floating-bilayer lipid membrane on a Au(111) surface modified with a hydrophilic monolayer[J]. Langmuir, 2011, 27(17): 10867-10877.

[23] Fa guy P W, Richmond W N. Real-time polarization modulation infrared spectroscopy applied to the study of water and hydroxide ions at electrode surfaces[J]. Journal of Electroanalytical Chemistry, 1996, 410(1): 109-113.

[24] Barth A. Infrared spectroscopy of proteins[J]. Biochimica et Biophysica Acta, 2007, 1767(9): 1073-1101.

[25] Vie V, Legardinier S, Chieze L, et al. Specific anchoring modes of two distinct dystrophin rod sub-domains interacting in phospholipid Langmuir films studied by atomic force microscopy and PM-IRRAS[J]. Biochimica et Biophysica Acta, 2010, 1798(8): 1503-1511.

[26] Brosseau C L, Leitch J, Bin X, et al. Electrochemical and PM-IRRAS a glycolipid-containing biomimetic membrane prepared using Langmuir-Blodgett/Langmuir-Schaefer deposition[J]. Langmuir, 2008, 24 (22): 13058-13067.

[27] Chen M, Li M, Brosseau C L, et al. AFM Studies of the effect of temperature and electric field on the structure of a DMPC-cholesterol bilayer supported on a Au(111) electrode surface[J]. Langmuir, 2009, 25(2): 1028-1037.

[28] Ohta Y, Yokoyama S, Sakai H, et al. Membrane properties of mixed ganglioside GM1/phosphatidylcholine monolayers[J]. Colloids and Surfaces B: Biointerfaces, 2004, 33(3/4): 191-197.

[29] Li N, Zamlynny V, Lipkowski J, et al. *In situ* IR reflectance absorption spectroscopy studies of pyridine adsorption at the Au(110) electrode surface[J]. Journal of Electroanalytical Chemistry, 2002, 43 (524-525): 43-53.

[30] Green M J, Barner B J, Corn R M. Real-time sampling electronics for double modulation experiments with Fourier transform infrared spectrometers[J]. Review of Scientific Instruments, 1991, 62(6): 1426-1430.

[31] Buffeteau T, Desbat B, Turlet J M. Polarization modulation FT-IR spectroscopy of surfaces and ultra-thin films: Experimental procedure and quantitative analysis[J]. Applied Spectroscopy, 1991, 45(3): 380-389.

[32] Buffeteau T, Desbat B, Blaudez D, et al. Calibration procedure to derive IRRAS spectra from PM-IRRAS spectra[J]. Applied Spectroscopy, 2000, 54(11): 1646-1650.

[33] Zamlynny V, Lipkowski J. Diffraction and spectroscopic methods in electrochemistry[M]//Alkire R, Kolb D M, Lipkowski J, et al. Ed. Weinheim: Wiley-VCH, 2006, 9: 315-376.

[34] Zamlynny V. PhD thesis[D]. University of Guelph, 2002.

[35] Palik E. Ed. Handbook of optical constants of solids II [M]. Academic Press: San Diego, 1998.

[36] Bertie J E, Ahmed M K, Eysel H H. Infrared intensities of liquids. 5. Optical and dielectric constants, integrated intensities, and dipole moment derivatives of H_2O and D_2O at 22 ℃[J]. The Journal of Physical Chemistry, 1989, 93(6): 2210-2218.

[37] Lipert R J, Lamp B D, Porter M D. Modern techniques in applied molecular spectroscopy[M]// Mirabella F M. Ed. New York: John Wiley & Sons, Inc., 1998: 83-126.

[38] Leonard A, Escrive C, Laguerre M, et al. Location of cholesterol in DMPC membranes. A comparative study by neutron diffraction and molecular mechanics simulation[J]. Langmuir, 2001, 17(6): 2019-2030.

[39] Li M, Chen M, Sheepwash E, et al. AFM studies of solid-supported lipid bilayers formed at a Au(111) electrode surface using vesicle fusion and a combination of Langmuir-Blodgett and Langmuir-Schaefer techniques [J]. Langmuir, 2008, 24(18): 10313-10323.

[40] Kycia A H, Sek S, Su Z F, et al. Electrochemical and STM Studies of 1-thio-β-d-glucose self-assembled on a Au(111) electrode surface[J]. Langmuir, 2011, 27(21): 13383-13389.

[41] Raguse B, Braach-Maksvytis V, Cornell B A, et al. Tethered lipid bilayer membranes: Formation and ionic reservoir characterization[J]. Langmuir, 1998, 14 (3): 648-659.

[42] Burgess I, Szymanski G, L, M, et al. Electric field-driven transformations of a supported model biological membrane—an electrochemical and neutron reflectivity study[J]. Biophysical Journal C, 2004, 86 (3): 1763-1776.

[43] Gennis R B. Biomembranes, molecular structure and function[M]. New York: Springer-Verlag, 1989.

[44] Liang C Y, Lytton M R. Infrared spectra of crystalline and stereoregular polymers[J]. Journal of Polymer Science, 1962, 61(172): S45-S48.

[45] Lee D C, Durrani, A A, Chapman D. A difference infrared spectroscopic study of gramicidin A, alamethicin and bacteriorhodopsin in perdeuterated dimyristoylphosphatidylcholine[J]. Biochimica et Biophysica Acta, 1984, 769(1): 49-65.

[46] Brosseau C L, Bin X, Roscoe S G, et al. Electrochemical and PM-IRRAS characterization of DMPC + choles-

terol bilayers prepared using Langmuir-Blodgett/Langmuir-Schaefer deposition[J] Journal of Electroanalytical Chemistry, 2008, 621(2): 222-228.

[47] Nabet A, Auger M, Pezolet M. Investigation of the temperature behavior of the bands due to the methylene stretching vibrations of phospholipid acyl chains by two-dimensional infrared correlation spectroscopy[J]. Applied Spectroscopy, 2000, 54(7): 948-955.

[48] Allara D L, Swalen J D. An infrared reflection spectroscopy study of oriented cadmium arachidate monolayer films on evaporated silver[J]. The Journal of Physical Chemistry, 1982, 86(14): 2700-2704.

[49] Allara D L, Nuzzo R G. Spontaneously organized molecular assemblies. 1. Formation, dynamics, and physical properties of *n*-alkanoic acids adsorbed from solution on an oxidized aluminum surface[J]. Langmuir, 1985, 1(1): 45-52.

[50] Bin X, Zawisza I, Lipkowski J. Electrochemical and PM-IRRAS studies of the effect of the static electric field on the structure of the DMPC bilayer supported at a Au(111) electrode surface[J]. Langmuir, 2005, 21(1): 330-347.

[51] Zawisza I, Bin X, Lipkowski J. Potential-driven structural changes in Langmuir-Blodgett DMPC bilayers determined by *in situ* spectroelectrochemical PM IRRAS [J]. Langmuir, 2007, 23(9): 5180-5194.

[52] Umemura J, Kamata T, Takenaka T. Quantitative evaluation of molecular orientation in thin Langmuir-Blodgett films by FT-IR transmission and reflection-absorption spectroscopy[J]. The Journal of Physical Chemistry, 1990, 94(1): 62-67.

[53] Hauser H, Pascher I, Pearson R H, et al. Preferred conformation and molecular packing of phosphatidylethanolamine and phosphatidylcholine [J]. Biochimica et Biophysica Acta, 1981, 650(1): 21-51.

[54] Aussenac F, Laguerre M, Schmitter J M, et al. Detailed structure and dynamics of bicelle phospholipids using selectively deuterated and perdeuterated labels. 2H NMR and molecular mechanics study[J]. Langmuir, 2003, 19(25): 10468-10479.

[55] Lewis R N A H, McElhaney R N. Components of the carbonyl stretching band in the infrared spectra of hydrated 1, 2-diacylglycerolipid bilayers: A reevaluation [J]. Biophysical Journal, 1994, 67(6): 2367-2375.

[56] Fringeli U P. The structure of lipids and proteins studied by attenuated total reflection (ATR) infrared spectroscopy. II. Oriented layers of a homologous series: Phosphatidylethanolamine to phosphatidylcholine[J]. Z Naturforsch C, 1977, 32(1/2): 20-45.

[57] Fringeli U P, Gunthard H H. Molecular biology, biochemistry and biophysics [M]. Grell E, Ed., Springer Verlag: Berlin, 1981: 270-332.

[58] Fringeli U P. A new crystalline phase of *L*-alpha-dipalmitoyl phosphatidylcholine monohydrate[J]. Biophysical Journal, 1981, 34(2): 173-1887.

[59] Hubner W, Blume A. Interactions at the lipid-water interface[J]. Chemistry and Physics of Lipids, 1998, 96 (1/2): 99-123.

金(111)电极表面浮动磷脂双层膜的原位偏振红外反射光谱研究

Zhangfei Su, Annia Kycia, J. Jay Leitch, Jacek Lipkowski*

(圭尔夫大学化学系, 加拿大 安大略省 N1G 2W1, 圭尔夫)

摘要: 应用电化学原位偏振红外反射光谱法研究了构建于金(111)电极表面的浮动磷脂双层膜. 金电极表面先自组装一层巯基葡萄糖单层来增加表面的亲水性,浮动磷脂双层膜通过 LB-LS 技术构建在巯基葡萄糖单层上. 双层膜由双肉豆蔻磷脂酰胆碱(DMPC)、胆固醇和神经节苷脂 GM1 构成. GM1 分子中的糖链可以物理吸附在巯基葡萄糖表面, 在双层膜和基底间形成一个富含水的隔层. 红外光谱表明浮动双层膜中的 DMPC 分子比传统的支撑双层膜中的 DMPC 分子有更强的水合作用, 证实了双层膜和基底间水层的存在. 该浮动双层膜更接近于实际的生物膜体系,并且在金电极表面有宽的电位区间,非常适于进一步的离子通道蛋白质研究.

关键词: 原位偏振红外反射光谱; 金(111)电极; 浮动磷脂双层膜